# Generation of Low-Dimensional Architectures through the Self-Assembly of Pyromellitic Diimide Derivatives

Chiara Musumeci, Monika Walęsa-Chorab, Adam Gorczyński, Grzegorz Markiewicz, Andrzej Bogucki, Roman Świetlik, Zbigniew Hnatejko, Wojciech Jankowski, Marcin Hoffmann, Emanuele Orgiu, et al.

ACS OMEGA

Article

http://pubs.acs.org/journal/acsodf

# Generation of Low-Dimensional Architectures through the Self-Assembly of Pyromellitic Diimide Derivatives

Chiara Musumeci,[†,⊥] Monika Wałęsa-Chorab,[‡] Adam Gorczyński,[‡] Grzegorz Markiewicz,[‡,§] Andrzej Bogucki,[∥] Roman Świetlik,[∥] Zbigniew Hnatejko,[‡] Wojciech Jankowski,[‡] Marcin Hoffmann,[‡] Emanuele Orgiu,[†] Artur R. Stefankiewicz,[‡,§] Violetta Patroniak,[‡] Artur Ciesielski,*[,†] and Paolo Samorì*[,†]

[†]Université de Strasbourg, CNRS, ISIS, 8 allée Gaspard Monge, 67000 Strasbourg, France

[‡]Faculty of Chemistry, Adam Mickiewicz University, Umultowska 89b, 61614 Poznań, Poland

[§]Centre for Advanced Technologies, Adam Mickiewicz University, Umultowska 89c, 61614 Poznań, Poland

[∥]Institute of Molecular Physics, Polish Academy of Sciences, Mariana Smoluchowskiego 17, 60-179 Poznań, Poland

Supporting Information

**ABSTRACT:** Small $\pi$-conjugated molecules can be designed and synthesized to undergo controlled self-assembly forming low-dimensional architectures, with programmed order at the supramolecular level. Such order is of paramount importance because it defines the property of the obtained material. Here, we have focused our attention to four pyromellitic diimide derivatives exposing different types of side chains. The joint effect of different noncovalent interactions including $\pi-\pi$ stacking, H-bonding, and van der Waals forces on the four derivatives yielded different self-assembled architectures. Atomic force microscopy studies, corroborated with infrared and nuclear magnetic resonance spectroscopic measurements, provided complementary multiscale insight into these assemblies.

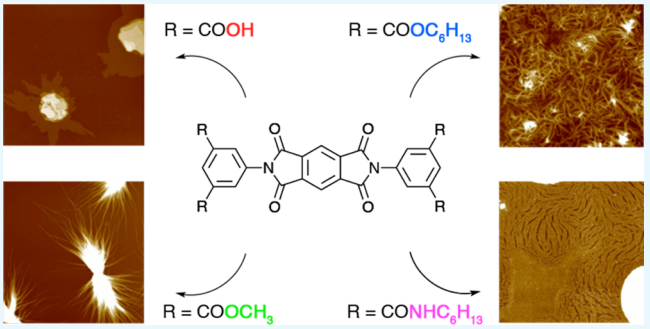


## INTRODUCTION

Molecular self-assembly at surfaces through the subtle control of the interplay between intramolecular, intermolecular, and interfacial interactions is a viable strategy to create highly ordered, supramolecularly engineered (multi)functional materials[1,2] as key components for the bottom-up fabrication of molecular-scale devices.[3−9]

$\pi$-Conjugated (small) molecules are capable of undergoing spontaneous self-assembly to form low-dimensional structures, which can efficiently transport charges and excitons.[10−18] Such systems have been investigated for their unique optical properties as dyes[19−22] and for their tendency to self-assemble into macroscopic supramolecular electroactive aggregates.[23] By modifying the experimental conditions and functionalization of the aromatic core, one can produce various types of aggregates such as nanowires,[24] nanoribbons,[25] and nanotubes.[26,27] These structures can be extremely useful and can be of interest for different technological applications in the field of organic photonics and electronics,[28,29] photovoltaics,[30,31] and sensing.[32] Among $\pi$-conjugated systems, rylene diimides are probably the most studied class of compounds, thanks to their versatility and ease of functionalization in different positions with a wide variety of substituents.[20,33−35]

In particular, pyromellitic diimide derivatives decorated with fluorinated side chains have been used as active layers in n-channel organic thin-film transistors, which show field-effect mobilities up to 0.079 $cm^2 V^{-1} s^{-1}$ and $I_{on}/I_{off}$ ratios of $10^6$.[36,37] These high performances result from the close $\pi-\pi$ stacking between the side benzene rings and pyromellitic diimide cores.[37] The mobility was almost one order of magnitude lower than that of the naphthalene diimide analogue,[35] primarily because of the smaller size of the aromatic core. The side N,N′-substituents were found to strongly influence the electrical characteristics of this material. This aspect, together with the relatively easy synthesis of pyromellitic diimide compared to that of other rylene derivatives, represents an advantage in terms of large-scale production, making these molecules interesting systems to be explored.

Recently, we have investigated the self-assembly of a pyromellitic diimide derivative, namely 5,5′-(1,3,5,7-tetraoxopyrrolo[3,4-*f*]isoindole-2,6-diyl)diisophthalic acid (**1**), forming a supramolecular two-dimensional (2D) network on highly oriented pyrolitic graphite (HOPG) substrates.[38] In that case, we found that H-bonding among adjacent carboxylic acid moieties was driving the self-assembly toward the formation of planar supramolecular architectures. The planar conformation

**Received:** March 10, 2017
**Accepted:** April 17, 2017
**Published:** April 26, 2017






DOI: 10.1021/acsomega.7b00286
*ACS Omega* 2017, 2, 1672−1678

of the molecule is in fact determined by the intramolecular C═O···H-C-H-bonds between the diimide core and the rylene substituents.

Although the H-bonding represents one of the most investigated noncovalent patterns,[39,40] in the present work we replace the carboxylic acids with other moieties to exploit other types of noncovalent interactions for modulating the self-assembly of pyromellitic diimide. In particular, we expand the capacity of these molecules to undergo self-assembly forming three-dimensional microscopic aggregates. Alongside the pyromellitic diimide functionalized with tetracarboxylic acid (**1**), we have focused our attention to two ester derivatives having $OCH_3$ (**2**) and $OC_6H_{13}$ (**3**) alkoxy groups and an $NHC_6H_{13}$ amide (**4**) moiety (Figure 1) (see Supporting Information (SI) for description of the synthesis).

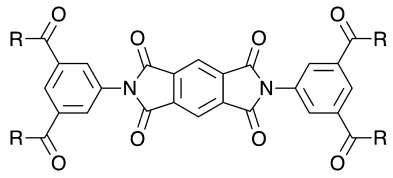


**Figure 1.** Molecular structure of the four pyromellitic diimides.

We have studied their molecular aggregation behavior by employing the solvent-induced precipitation (SIP) approach,[41,42] followed by a slow post-treatment process, that is, solvent vapor annealing (SVA),[43,44] which was expected to promote rearrangement of the obtained architectures on the solid substrate. The self-assembly behavior was also explored by means of atomic force microscopy (AFM) corroborated by $^1$H NMR and temperature-resolved IR studies.

## RESULTS AND DISCUSSION

A drop of 0.1 mM solution of compounds **1**−**4** was applied to the basal plane of $SiO_2$ substrates. Because of their low solubility, compounds **1** and **2** were dissolved in warm dimethyl sulfoxide (DMSO), whereas **3** and **4** were solubilized in chloroform. To promote molecular aggregation, SIP was exploited by adding aliquots of 1:50 v/v ratio of solutions in a nonsolvent. The chosen nonsolvent was chloroform for compounds **1** and **2** and methanol for compounds **3** and **4**. The obtained dispersions (50 $\mu$L) were drop-casted onto $SiO_2$ substrates and dried in air.

The morphology of the films obtained by fast aggregation process induced by the addition of a nonsolvent during SIP was imaged by AFM operating in intermittent contact-mode (Figure 2a−d). In such an SIP process, the molecule−molecule interactions are maximized and the substrate has mainly the role of guiding the positioning of structures already preformed.

Figure 2a reveals that compound **1** forms $\mu$m-thick aggregates on $SiO_2$ as a result of the poor wettability of the dropped dispersion, which tends to cluster in very small regions on $SiO_2$. Nevertheless, by investigating the apparently uncovered areas, very small and flat regions of a molecular adsorbate are observed. These domains are homogeneously spread on the surface of $SiO_2$: they consist of grains exhibiting an average thickness of 1 nm and diameters of about 150 nm (see the inset in Figure 2a and the particle distribution in Figure S10), which is consistent with a self-assembly scenario in which molecules are arranged in an edge-on fashion.

Interestingly, when the pyromellitic diimides are decorated with different side chains, they exhibit markedly different SIP-induced assembly behaviors. Bundles of crystal-like needles were, in fact, observed in the two ester derivatives, that is, **2** and **3**, whereas compound **4** was found to form more flexible fiberlike structures. The size of the fibers was also estimated from the AFM images. Compound **2** formed fibers of 5−10 $\mu$m

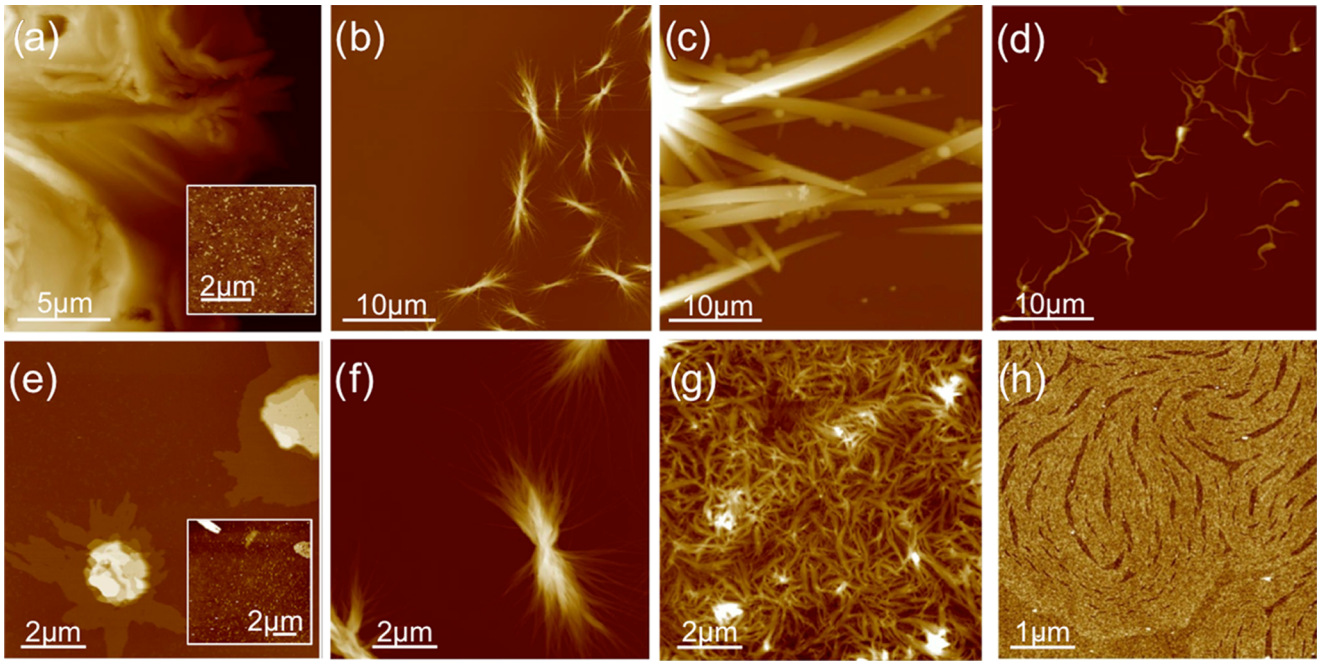


**Figure 2.** Topographical AFM images of the self-assembled architectures produced by SIP (top) and their successive modification resulted from the SVA post-treatment (bottom) of compounds **1** (a, e), **2** (b, f), **3** (c, g), and **4** (d, h). *Z*-scales: (a) 3 $\mu$m (inset: 4 nm), (b) 600 nm, (c) 3 $\mu$m, (d) 1000 nm, (e) 80 nm (inset: 7 nm) (f) 900 nm, (g) 80 nm, and (h) 3 nm.



DOI: 10.1021/acsomega.7b00286
*ACS Omega* 2017, 2, 1672−1678

in length, with the thinnest fibers having a diameter of 1.2−1.5 nm. The structures formed from compound **3** were several tens of micrometers in length and hundreds-of-nanometer wide. Finally, the fibers of compound **4** were a few micrometers long and tens of nanometer wide (see more details in Figure S14).

In the employed SIP deposition process, the aggregates previously formed in solution are transferred onto the substrate surface. This phenomenon was indeed confirmed by depositing the solution of **1** on mica, showing sheetlike structures (observed also in $SiO_2$) yet in this case oriented along preferential directions, reflecting the 3-fold symmetry of the crystalline substrate (see Figure S10).

In the second stage, all of the samples of Figure 2a−d were kept in a sealed environment saturated with the vapors of $CHCl_3$ to promote structural rearrangement onto the surface; the results of this post-processing are shown in Figure 2e−h. The acid derivative **1**-based, micrometer-thick aggregates rearrange into layered architectures, even though the thicker, small sheetlike structures are still present.

By carefully measuring the thickness of the layers from profiles in AFM topographical images, it was noticed that they are multiples of 1.3 nm, which corresponds to a configuration where the molecules are standing in an edge-on configuration on the substrate (see Figure S11).

Although the SIP-produced aggregates of compound **2** seem not to be affected by the SVA post-treatment (Figure 2b vs Figure 2f), the morphologies of the films of **3** and **4** appear to change dramatically after exposure to the solvent vapors. In particular, the rigid crystal-like needles of **3** observed in Figure 2c reorganize at surfaces forming an intricate layer of flexible fibrillar structures (Figure 2g). Conversely, the already flexible hundreds-of-nanometer tall structures of **4** shown in Figure 2d seem to establish a stronger interaction with the substrate, by forming a layer around 1 nm thick, which is noticeably composed by very long fibrillar structures assembled in a uniform fashion (Figure 2h). By analyzing the thickness of these fibrils, it is possible to deduce that the layer is a monomolecular one, where the fibrils are composed of molecules stacked, with their long axis likely parallel to the substrate. Such an assembly can be described by the formation C═O···H−N bonds formed between the amide moieties and $\pi-\pi$ interactions between the aromatic cores. The labile nature of the molecular assemblies of **3** and **4** can be attributed to the formation of thermodynamically favored structures upon exposure to chloroform vapors, during which the assemblies formed through the SIP process are rearranged to maximize both molecule−molecule and molecule−substrate interactions.

The self-assembly behavior of these molecules in solution has been studied by NMR (see Figures S2−S9). Although the NMR spectra of derivatives **2** and **3** showed no evidence of intermolecular interactions, derivatives **1** and **4** were found to create intermolecular H-bonds. On one hand, NMR studies of **1** have been already reported.[38] On the other hand, NMR spectra of **4** in DMSO-$d_6$, being an exceptionally strong H-bond acceptor, display signals expected for compound **4** (Figures S6 and S7). In such a solvent, any intermolecular (and intramolecular) H-bonds are completely disrupted, leading to solvated monomers, in which any conformational interconversion is sufficiently fast to lead to the expected $C_2$ symmetry on the NMR chemical shift timescale. Conversely, the $^1$H NMR spectrum of compound **4** in $CDCl_3$ (Figure S8), being a solvent that does not disrupt intermolecular (or intramolecular) H-bonding, is significantly different and entirely consistent with the formation of a H-bonded structure. The latter is evidenced by the broadening of the NMR resonance lines (see signals NH and CH at 6.38 and 8.48 ppm, respectively) in stark contrast to the spectrum obtained in DMSO-$d_6$. Variable temperature $^1$H NMR spectra of compound **4** in the 233−323 K temperature range in $CDCl_3$ were recorded to gain insight into the self-assembly of **4** in solution (Figure S9). Upon heating the sample up to 323 K, a significant sharpening and shifting of the two resonance lines engaged in the formation of the supramolecular assembly is monitored. Such observations can be ascribed to the progressive degradation of the H-bonding interactions. By lowering the temperature of the sample, a significant broadening of proton signals was monitored up to 273 K, which can be associated with increased participation to hydrogen bonds between the molecules and/or formation of stacking assemblies. Interestingly, below 253 K, the spectra become very complex, showing multiple splitting of the resonance lines, which is probably a sign of the formation of higher order aggregates. Structural behavior of different compounds is well known to be dependent on solvation energies and intermolecular interactions, thus giving rise to question whether the molecular assemblies present in the solid state accurately reflect those existing in solution. Herein, we propose that the fibrillar architectures observed in the solid state by AFM might not necessarily be the dominant species in solution, especially at lowered temperatures. Bearing in mind that the strength of the intermolecular interactions, that is, (i) H-bonding, (ii) $\pi-\pi$ stacking, and (iii) alkyl-chain interdigitation generally can be described as (i) ≫ (ii) ≅ (iii), we speculate that a decrease in temperature facilitates face-to-face aggregation of aromatic diimide cores, some of which might interact with each other via intermolecular H-bonding in such a way that finally even alkyl chains become ordered to a certain extent.

To probe interactions in the solid state between individual pyromellitic diimide derivatives **1**−**4**, IR spectra were recorded for their powder and thin film forms (see Experimental Procedures) at variable temperatures, thus focusing our attention on the groups which can noncovalently interact, that is, the C═O, C−H, and O−H moieties. The stretching modes of these groups yield strong IR bands that are well separated from other vibrational bands; therefore, they are especially suitable for our considerations.

Compound **1** was not found to melt. Above ca. 230 °C, the samples gradually and irreversibly changed their color, providing evidence for the occurrence of decomposition. In particular, we have visualized a broad spectral feature in the wavenumber range 2100−3700 $cm^{-1}$ which can be ascribed to stretching modes of hydrogen bonded O−H groups and consists of at least three components centered at about 3560, 2980, and 3480 $cm^{-1}$ (Figure 3a). Because **1** has four carboxylic groups related to each other by $C_2$ symmetry, it is possible that the molecules in the crystal are interacting via O−H···O bridges (Figure 3b) to form 2D arrays, similarly to those previously observed on the HOPG substrate.[38] The absence of any vibrational feature at ca. 3650 $cm^{-1}$ indicates that all carboxylic groups are involved in H-bonds. Interactions between individual 2D layers are also possible, thus leading to the generation of larger aggregates, likely via $\pi-\pi$ stacking. With the increasing temperature, the intensity of the broad 2100−3700 $cm^{-1}$ feature considerable decreases but without any significant change of the band shape. The only visible modification is noticed for the component at ca. 3480 $cm^{-1}$. This relatively broad component at 25 °C disappears upon



DOI: 10.1021/acsomega.7b00286
ACS Omega 2017, 2, 1672−1678

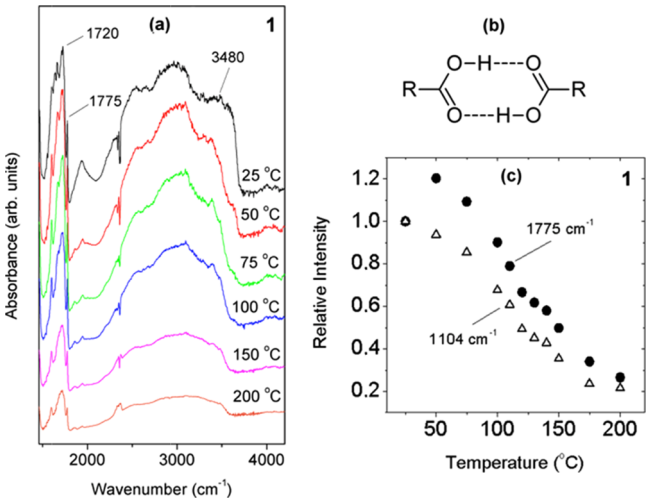


**Figure 3.** (a) Temperature dependence of the IR spectra of **1** (powder); (b) schematic representation of −COOH dimer; (c) integral intensity of the bands at 1775 $cm^{-1}$ (filled circles) and 1104 $cm^{-1}$ (triangles).

heating at about 50 °C; however, at higher temperatures a much narrower band at the same position is observed. We propose that at room temperature two kinds of the O−H···O bond (intramolecular and intermolecular) exist that are responsible for formation of two kinds of intralayer hydrogen bonding motifs shown schematically in Figure S15 as MODE A and MODE B. MODE A is ascribed to the form of the previously observed H-bonding pattern,[38] where each COOH group of **1** interacts with four neighboring molecules through the formation of four complementary di-hapto H-bonds. MODE B has been attributed to the pattern in which each carboxylic group contributes to the formation of a single H-bond with diimide carbonyl group, which are not involved in the pattern in MODE A, and one intermolecular C═O···H interaction. Upon heating to about 50 °C, molecule **1** was found to undergo rearrangement from MODE B to MODE A, and the O−H band at 3480 $cm^{-1}$ related to the intramolecular H-bond nearly disappeared. In the region of C═O stretching vibrations, we find a band at about 1775 $cm^{-1}$ that can be assigned to the free C═O (not involved in H-bonds) belonging to the imide groups of **1**. On the other hand, a broad band centered at about 1720 $cm^{-1}$, which consists of several components, is attributed to the C═O groups (both imide and carboxylic) which form H-bonds. With the increasing temperature, it is possible to observe a continuous decrease in intensity of the C═O feature at 1720 $cm^{-1}$, similar to the observation for the O−H bands. At the same time, the intensity of the band at 1775 $cm^{-1}$ grows up to about 50 °C and above this temperature it decreases (Figure 3c); the temperature behavior of this band is different in comparison with other vibrational features of **1**, for example, the band at 1104 $cm^{-1}$ (Figure 3c). By and large, within the proposed interpretation, the temperature behavior of both O−H and C═O bands suggests that heating-induced transition from MODE B to MODE A takes place and is followed by continuous decomposition of the latter mode upon further heating.

Compound **2** melts above ca. 360 °C; the relatively high melting temperature can be determined by the occurrence of $\pi-\pi$ stacking between the aromatic rings of molecules and the absence of both long alkyl chains and H-bonding. Temperature dependence of the IR spectra of the sample heated up to melting is shown in Figure S16a. The band intensities gradually decrease with the temperature but without any important modifications, which could indicate a phase transition. After sample melting a thin film was formed. The IR spectra of such a thin film upon cooling down to 25 °C and then heating up to 370 °C were practically the same (Figure S16b). Before crystal heating at 25 °C in the region of C−H stretching, we find three bands at 2964, 3027, and 3090 $cm^{-1}$, which are due to the methyl groups and aromatic moieties. The bands at 3490 and 3587 $cm^{-1}$ can be assigned to overtones of the C═O stretching mode; it is also possible that they are due to water molecules present in the crystal of **2**. At 1730 $cm^{-1}$, strong vibrational feature can be seen and can be attributed to the C═O stretching vibrations from ester groups, and at 1775 $cm^{-1}$, a weaker and narrower band attributed to C═O stretching of free imide moieties groups can be seen. The band at 1775 $cm^{-1}$ gets slightly stronger in film.

Melting of compound **3** was observed at about 160 °C. In the spectra recorded at room temperature, the bands at 2861, 2926, 2950, and 3082 $cm^{-1}$ can be attributed to the C−H stretching modes of alkyl and aromatic rings, whereas the bands at 3254 and 3485 $cm^{-1}$ are most probably overtones of the C═O mode and/or water molecules (see Figure S17a). Within the region of C═O stretching, we observe two bands at 1710 and 1732 $cm^{-1}$, which by analogy with **1** and **2** could be assigned to associated C═O groups; it is remarkable that this spectrum does not exhibit a well-defined spectral feature, which could be attributed to the free C═O groups. We propose those to be a result of the disordered nature of individual molecules with regard to self-assembly in the solid state, allowing for CH···O═C contacts responsible for the observed wavenumber values. After melting and recrystallization, the IR spectra undergo considerable changes, which give evidence of formation of a new phase. In this case, we observe both the free C═O bonds of imide groups and the C═O bonds of end groups, which can be at least partially associated, yielding bands at 1720 and 1772 $cm^{-1}$, respectively (Figure S17b). In the new phase also, the C−H stretching bands are more narrow and easy to be recognized. By and large, after recrystallization, the sample gets more ordered; nevertheless, in this phase, the C═O bonds are not involved in H-bond contacts. We tentatively propose that upon the occurrence of heating and cooling cycles molecule **3** self-assembles into structures exhibiting a higher degree of order, which involves both interdigitation of alkyl chains and $\pi-\pi$ stacking interactions, the latter occurs in the steplike manner (Figure S18). Such phenomena would be in accordance with AFM studies and could explain that molecule−substrate interactions are weaker than mutual molecule−molecule interactions. Because the only difference within the framework of compounds **2** and **3** involves the length of the alkyl chain (methyl for **2** and *n*-hexyl for **3**), additional conclusions can be drawn. Apart from a significant increase in the melting temperature of **2**, it seems that the main consequence of tuning the length of the ester chain is an increase of the degree of conformational freedom, as observed during heating/melting/cooling cycle of **3**. Importantly, similar behavior was not observed for **2**, because hardly any changes were noticed upon applying the same experimental protocol.

Compound **4** melts at ca. 250 °C. At 25 °C, the IR spectrum of **4** reveals a group of strong bands centered at 2920 $cm^{-1}$ (superposition of three components at 2866, 2920, 2959 $cm^{-1}$), which can be attributed to the C−H stretching modes of alkyl



DOI: 10.1021/acsomega.7b00286
ACS Omega 2017, 2, 1672−1678

$-(CH_2)_5CH_3$ groups (Figure 4a). The band at 3073 $cm^{-1}$ is assigned to the C−H stretching of aromatic rings. The

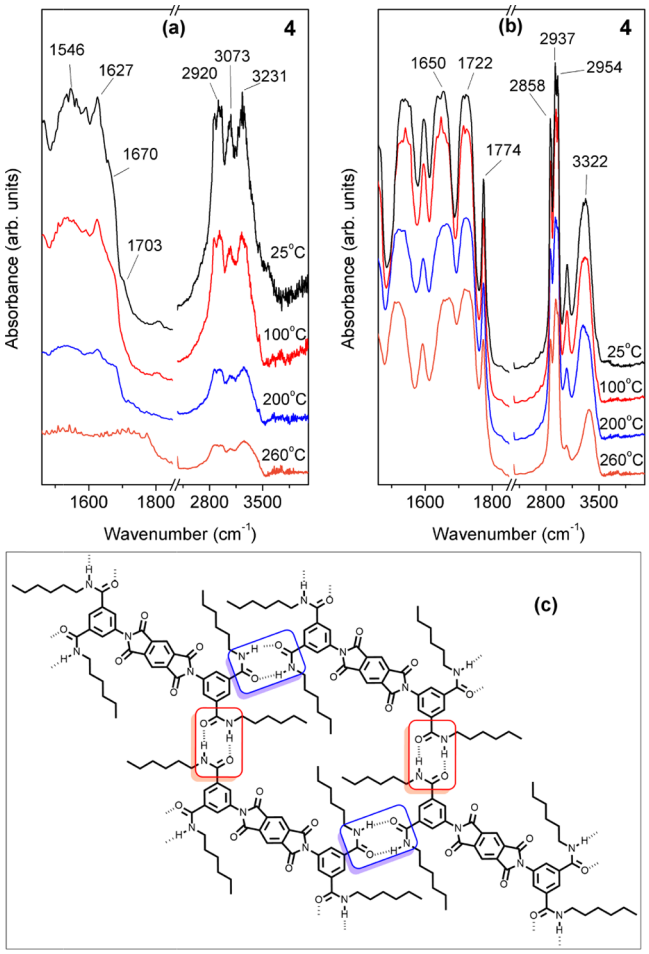


**Figure 4.** Temperature dependence of IR spectra of **4** recorded on (a) powder and (b) thin film. In both cases, the samples were heated until melting. (c) Schematic representation of the proposed stable, H-bonded, and self-assembled structure of compound **4** observed upon cooling.

considerable bandwidth of the C−H bands provides evidence of a disorder of the alkyl groups. The band centered at 3231 $cm^{-1}$ is due to N−H groups, which form H-bonds. Surprisingly, the C═O modes of both the free and associated groups are not observed (or nearly not observable). When the temperature increases up to sample melting, the intensity of all vibrational bands decreases. After cooling the film, IR spectra are considerably modified; the spectra and their temperature dependence are very similar to those subsequently obtained by heating of the thin film (Figure 4b). At 25 °C, one can observe quite narrow bands at 2858, 2937, 2954, and 3078 $cm^{-1}$ assigned to the C−H stretching and the band at 3322 $cm^{-1}$ assigned to the stretching of N−H groups involved into the H-bonds.

The absence of any bands at higher frequencies, which could be related to free N−H groups, proves that all the groups form H-bonds. In the case of thin films, we clearly see bands due to C═O stretching at 1774 $cm^{-1}$ related to free groups and at 1722 $cm^{-1}$ related to groups forming H-bonds of the type N−H···O (proposed form of compound **4** is shown in Figure 4c). We suggest that in the original sample before melting the C═O vibrational features are covered with the strong and broad N−H bending feature at 1627 $cm^{-1}$, and they are only evident as weak shoulders at 1670 and 1703 $cm^{-1}$ (Figure 4a). In conclusion, the disorder disappears due to compound recrystallization from melt leading to a new phase of **4**, which could be associated with the aggregates observed with AFM after the SVA step.

The charge transport properties of all of the synthesized compounds were tested in field-effect transistors devices and described in the SI. All of the tested compounds, except **1**, did not exhibit any semiconducting behavior. This result can be possibly ascribed to an unfavorable molecular packing of compounds **2**, **3**, and **4**, which could hinder the charge transport. This interpretation was further supported by density functional theory (DFT) calculations taking into account solvation model (PCM) revealing that the HOMO/LUMO energy gaps in DMSO and DCM for compounds **2**−**3** had similar values of ca. 4.3 eV, whereas for compounds **1** and **4** the HOMO/LUMO energy gaps were slightly smaller (Table S2 and Figure S20), which translates in a lower charge transport ability for such derivatives.

## CONCLUSIONS

We have designed and synthesized four pyromellitic diimide derivatives exposing the different types of side chains to explore their ability of undergoing self-assembly through diverse noncovalent interactions, forming ordered architectures. A comparative AFM study revealed that all derivatives undergo self-assembly on the solid substrates to form different low-dimensional aggregates. Further information about their self-assembly behavior was acquired from temperature-dependent IR spectroscopy and NMR solution studies. In particular, we found that tetracarboxylic acid derivative **1** forms small monomolecular-thick 2D crystals in a self-assembly process primarily governed by H-bonding and $\pi-\pi$ stacking. Interestingly, by introducing different side chains to the pyromellitic diimide core, the SIP-induced assembly changes dramatically. Bundles of crystal-like needles are in fact observed for the two esters derivatives, that is, pyromellitic diimide functionalized with $OCH_3$ (**2**) and $OC_6H_{13}$ (**3**), whereas more flexible fiberlike structures are observed for the amide derivative equipped with $NHC_6H_{13}$ side chains (**4**). The formation of such fibrillar structures has been primarily determined by the stacking between molecules (for **2** and/or **3**), and intermolecular N−H···O═C−H-bonds (for **4**). This study demonstrates that functionalization of pyromellitic diimide derivatives with specific side groups can be used to modify and control the morphology of the supramolecular aggregates on the solid surface, which could be potentially employed for tuning the self-assembly of other molecules with high affinity for $\pi-\pi$ stacking, which is highly desirable for low-cost large-area organic electronics. In addition, monitoring the morphological changes on the large-scale supramolecular assemblies can represent an interesting approach for the elucidation of biological nanosystems or construction of sensory devices.

## EXPERIMENTAL PROCEDURES

Synthesis of the compounds **1**−**4** has been described in the SI.

AFM morphological characterization was performed in intermittent contact-mode in a Dimension 3100 microscope equipped with a Nanoscope IV controller (Digital Instruments). Commercial silicon cantilevers with a nominal spring



DOI: 10.1021/acsomega.7b00286
ACS Omega 2017, 2, 1672−1678

constant of 40 N $m^{-1}$ were used for morphological characterization in tapping mode. Drops of 0.1 mM solutions of compounds **1**−**4** were applied to the $SiO_2$ substrates. To induce a fast aggregation, SIP was exploited by adding aliquots of 1:50 v/v ratio of solutions in a nonsolvent. In particular, the nonsolvent for compounds **1** and **2** was chloroform, whereas for compounds **3** and **4**, it was methanol. The obtained dispersions (50 $\mu$L) were drop-casted onto the $SiO_2$ substrates and dried in air.

NMR spectra were recorded on the Bruker Fourier 300 MHz (5 mm Fourier $^{1}H/^{13}C$ probe) and Bruker 400 MHz Avance III HD (5 mm BBFO probe) spectrometers, with standard Bruker pulse sequences. Spectra were referenced on the solvent residual peaks. NMR solvents were purchased from Euriso-Top or Deutero GmbH and used as received.

Infrared (IR) absorption spectra were studied within the mid-IR range (400−4000 $cm^{-1}$) by using a Bruker Equinox 55 FTIR spectrometer equipped with a KBr beam splitter. For temperature measurements, the samples were placed on a KBr plate in a THMS 600 Linkam heating stage equipped with a temperature controller. Initially, the samples in the form of powders were studied at room temperature. Subsequently, they were heated until melting to obtain thin films (**1**, decomposition without melting >230 °C; **2**, mp >360 °C; **3**, mp >160 °C; **4**, mp >250 °C), which were then cooled down and reheated again. Each temperature cycle was performed in a temperature range between room temperature and the temperature above melting point. During such cycles, IR spectra were continuously collected. The sample melting was visually observed using an optical microscope and in this way the melting temperature was determined. The rate of sample cooling/heating was about 2 °C/min.

## ■ ASSOCIATED CONTENT

### Supporting Information

The Supporting Information is available free of charge on the ACS Publications website at DOI: 10.1021/acsomega.7b00286.

Synthetic details of compounds **2**−**4**; DFT data; UV/vis spectra of compounds **2**−**4**; temperature-dependent FTIR spectra; VT NMR spectra of compound **4**; charge transport properties of all derivatives were tested in field-effect transistor devices (PDF)

## ■ AUTHOR INFORMATION


### Corresponding Authors

*E-mail: ciesielski@unistra.fr (A.C.).
*E-mail: samori@unistra.fr (P.S.).

### ORCID

Chiara Musumeci: 0000-0001-7923-8086
Monika Wałęsa-Chorab: 0000-0002-0605-6078
Emanuele Orgiu: 0000-0002-8232-0950
Paolo Samorì: 0000-0001-6256-8281

### Present Address

⊥NUANCE Center, Northwestern University, Silverman Hall, 2170 Campus Drive, Evanston, Illinois 60208-3113, United States (C.M.).


### Author Contributions

The manuscript was written through contributions of all authors. All authors have given approval to the final version of the manuscript.

### Notes

The authors declare no competing financial interest.

## ■ ACKNOWLEDGMENTS

This work was financially supported by the ERC project SUPRAFUNCTION (GA-257305), the EC Marie-Curie projects ITN iSwitch (GA no. 642196), the Agence Nationale de la Recherche through the LabEx project Chemistry of Complex Systems (ANR-10-LABX-0026_CSC), the International Center for Frontier Research in Chemistry (icFRC), National Science Centre (Grant no. 2015/18/E/ST5/00188), National Center for Research and Development (LIDER - 024/391/L-5/13/NCBR/2014), Polish Ministry of Science and Higher Education: IUVENTUS PLUS (0446/IP3/2015/73), and Grant no. 0111/DIA/2012/41 in the frame of "Diamond Grant" program and the PL-Grid Infrastructure. A.G. is a scholarship holder: (i) funded by the Polish National Science Center (Grant no. 2016/20/T/ST5/00187) in the frame of ETIUDA program, (ii) within the project "Scholarship support for Ph.D. students specializing in majors strategic for Wielkopolska's development", Sub-measure 8.2.2 Human Capital Operational Programme, co-financed by the European Union under the European Social Fund.

## ■ REFERENCES


(1) Whitesides, G. M.; Grzybowski, B. Self-assembly at all scales. *Science* **2002**, *295*, 2418−2421.
(2) Palma, C.-A.; Cecchini, M.; Samorì, P. Predicting self-assembly: from empirism to determinism. *Chem. Soc. Rev.* **2012**, *41*, 3713−3730.
(3) Balzani, V.; Credi, A.; Raymo, F. M.; Stoddart, J. F. Artificial molecular machines. *Angew. Chem., Int. Ed.* **2000**, *39*, 3349−3391.
(4) Kay, E. R.; Leigh, D. A.; Zerbetto, F. Synthetic molecular motors and mechanical machines. *Angew. Chem., Int. Ed.* **2007**, *46*, 72−191.
(5) Pérez-García, L.; Amabilino, D. B. Spontaneous resolution, whence and whither: from enantiomorphic solids to chiral liquid crystals, monolayers and macro- and supra-molecular polymers and assemblies. *Chem. Soc. Rev.* **2007**, *36*, 941−967.
(6) Gomar-Nadal, E.; Puigmarti-Luis, J.; Amabilino, D. B. Assembly of functional molecular nanostructures on surfaces. *Chem. Soc. Rev.* **2008**, *37*, 490−504.
(7) De Greef, T. F. A.; Smulders, M. M. J.; Wolffs, M.; Schenning, A. P. H. J.; Sijbesma, R. P.; Meijer, E. W. Supramolecular Polymerization. *Chem. Rev.* **2009**, *109*, 5687−5754.
(8) Gillissen, M. A. J.; Koenigs, M. M. E.; Spiering, J. J. H.; Vekemans, J. A. J. M.; Palmans, A. R. A.; Voets, I. K.; Meijer, E. W. Triple Helix Formation in Amphiphilic Discotics: Demystifying Solvent Effects in Supramolecular Self-Assembly. *J. Am. Chem. Soc.* **2014**, *136*, 336−343.
(9) Palmans, A. R. A.; Meijer, E. W. Amplification of chirality in dynamic supramolecular aggregates. *Angew. Chem., Int. Ed.* **2007**, *46*, 8948−8968.
(10) De Luca, G.; Pisula, W.; Credgington, D.; Treossi, E.; Fenwick, O.; Lazzerini, G. M.; Dabirian, R.; Orgiu, E.; Liscio, A.; Palermo, V.; Müllen, K.; Cacialli, F.; Samorì, P. Non-conventional Processing and Post-processing Methods for the Nanostructuring of Conjugated Materials for Organic Electronics. *Adv. Funct. Mater.* **2011**, *21*, 1279−1295.
(11) Briseno, A. L.; Mannsfeld, S. C. B.; Reese, C.; Hancock, J. M.; Xiong, Y.; Jenekhe, S. A.; Bao, Z.; Xia, Y. N. Perylenediimide nanowires and their use in fabricating field-effect transistors and complementary inverters. *Nano Lett.* **2007**, *7*, 2847−2853.
(12) Mas-Torrent, M.; Rovira, C. Novel small molecules for organic field-effect transistors: towards processability and high performance. *Chem. Soc. Rev.* **2008**, *37*, 827−838.
(13) Minder, N. A.; Ono, S.; Chen, Z. H.; Facchetti, A.; Morpurgo, A. F. Band-Like Electron Transport in Organic Transistors and




DOI: 10.1021/acsomega.7b00286
*ACS Omega* 2017, 2, 1672−1678

Implication of the Molecular Structure for Performance Optimization. *Adv. Mater.* **2012**, *24*, 503−508.
(14) Hoeben, F. J.; Jonkheijm, P.; Meijer, E. W.; Schenning, A. P. H. J. About supramolecular assemblies of pi-conjugated systems. *Chem. Rev.* **2005**, *105*, 1491−1546.
(15) Elemans, J. A. A. W.; Van Hameren, R.; Nolte, R. J. M.; Rowan, A. E. Molecular materials by self-assembly of porphyrins, phthalocyanines, and perylenes. *Adv. Mater.* **2006**, *18*, 1251−1266.
(16) Mativetsky, J. M.; Orgiu, E.; Lieberwirth, I.; Pisula, W.; Samorì, P. Charge Transport Over Multiple Length Scales in Supramolecular Fiber Transistors: Single Fiber Versus Ensemble Performance. *Adv. Mater.* **2014**, *26*, 430−435.
(17) Musumeci, C.; Salzmann, I.; Bonacchi, S.; Röthel, C.; Duhm, S.; Koch, N.; Samorì, P. The Relationship between Structural and Electrical Characteristics in Perylenecarboxydiimide-Based Nanoarchitectures. *Adv. Funct. Mater.* **2015**, *25*, 2501−2510.
(18) Rekab, W.; Stoeckel, M. A.; El Gemayel, M.; Gobbi, M.; Orgiu, E.; Samorì, P. High-Performance Phototransistors Based on PDIF-CN2 Solution-Processed Single Fiber and Multifiber Assembly. *ACS Appl. Mater. Interfaces* **2016**, *8*, 9829−9838.
(19) Magalhaes, J. L.; Pereira, R. V.; Triboni, E. R.; Berci, P.; Gehlen, M. H.; Nart, F. C. Solvent effect on the photophysical properties of 4-phenoxy-N-methyl-1,8-naphthalimide. *J. Photochem. Photobiol., A* **2006**, *183*, 165−170.
(20) Weil, T.; Vosch, T.; Hofkens, J.; Peneva, K.; Müllen, K. The Rylene Colorant Family-Tailored Nanoemitters for Photonics Research and Applications. *Angew. Chem., Int. Ed. Engl.* **2010**, *49*, 9068−9093.
(21) Peneva, K.; Mihov, G.; Nolde, F.; Rocha, S.; Hotta, J.; Braeckmans, K.; Hofkens, J.; Uji-I, H.; Herrmann, A.; Müllen, K. Water-soluble monofunctional perylene and terrylene dyes: Powerful labels for single-enzyme tracking. *Angew. Chem., Int. Ed. Engl.* **2008**, *47*, 3372−3375.
(22) Flors, C.; Oesterling, I.; Schnitzler, T.; Fron, E.; Schweitzer, G.; Sliwa, M.; Herrmann, A.; van der Auweraer, M.; de Schryver, F. C.; Müllen, K.; Hofkens, J. Energy and electron transfer in ethynylene bridged perylene diimide multichromophores. *J. Phys. Chem. C* **2007**, *111*, 4861−4870.
(23) Chen, Z.; Lohr, A.; Saha-Möller, C. R.; Würthner, F. Self-assembled pi-stacks of functional dyes in solution: structural and thermodynamic features. *Chem. Soc. Rev.* **2009**, *38*, 564−584.
(24) Schenning, A. P. H. J.; Meijer, E. W. Supramolecular electronics; nanowires from self-assembled pi-conjugated systems. *Chem. Commun.* **2005**, 3245−3258.
(25) Samorì, P.; Francke, V.; Müllen, K.; Rabe, J. P. Self-assembly of a conjugated polymer: from molecular rods to a nanoribbon architecture with molecular dimensions. *Chem. − Eur. J.* **1999**, *5*, 2312−2317.
(26) Hill, J. P.; Jin, W. S.; Kosaka, A.; Fukushima, T.; Ichihara, H.; Shimomura, T.; Ito, K.; Hashizume, T.; Ishii, N.; Aida, T. Self-assembled hexa-peri-hexabenzocoronene graphitic nanotube. *Science* **2004**, *304*, 1481−1483.
(27) Röger, C.; Müller, M. G.; Lysetska, M.; Miloslavina, Y.; Holzwarth, A. R.; Würthner, F. Efficient energy transfer from peripheral chromophores to the self-assembled zinc chlorin rod antenna: A bioinspired light-harvesting system to bridge the "green gap". *J. Am. Chem. Soc.* **2006**, *128*, 6542−6543.
(28) Würthner, F.; Schmidt, R. Electronic and crystal engineering of acenes for solution-processible self-assembling organic semiconductors. *ChemPhysChem* **2006**, *7*, 793−797.
(29) Zhang, L.; Zhong, X.; Pavlica, E.; Li, S.; Klekachev, A.; Bratina, G.; Ebbesen, T. W.; Orgiu, E.; Samorì, P. A nanomesh scaffold for supramolecular nanowire optoelectronic devices. *Nat. Nanotechnol.* **2016**, *11*, 900−906.
(30) Brabec, C. J.; Sariciftci, N. S.; Hummelen, J. C. Plastic solar cells. *Adv. Funct. Mater.* **2001**, *11*, 15−26.
(31) Schmidt-Mende, L.; Fechtenkötter, A.; Müllen, K.; Moons, E.; Friend, R. H.; MacKenzie, J. D. Self-organized discotic liquid crystals for high-efficiency organic photovoltaics. *Science* **2001**, *293*, 1119−1122.
(32) Squillaci, M. A.; Ferlauto, L.; Zagranyarski, Y.; Milita, S.; Müllen, K.; Samorì, P. Self-Assembly of an Amphiphilic pi-Conjugated Dyad into Fibers: Ultrafast and Ultrasensitive Humidity Sensor. *Adv. Mater.* **2015**, *27*, 3170−3174.
(33) Suraru, S. L.; Würthner, F. Strategies for the Synthesis of Functional Naphthalene Diimides. *Angew. Chem., Int. Ed. Engl.* **2014**, *53*, 7428−7448.
(34) Anthony, J. E.; Facchetti, A.; Heeney, M.; Marder, S. R.; Zhan, X. W. n-Type Organic Semiconductors in Organic Electronics. *Adv. Mater.* **2010**, *22*, 3876−3892.
(35) Zhan, X.; Facchetti, A.; Barlow, S.; Marks, T. J.; Ratner, M. A.; Wasielewski, M. R.; Marder, S. R. Rylene and Related Diimides for Organic Electronics. *Adv. Mater.* **2011**, *23*, 268−284.
(36) Kola, S.; Tremblay, N. J.; Yeh, M. L.; Katz, H. E.; Kirschner, S. B.; Reich, D. H. Synthesis and Characterization of a Pyromellitic Diimide-Based Polymer with C- and N-Main Chain Links: Matrix for Solution-Processable n-Channel Field-Effect Transistors. *ACS Macro Lett.* **2012**, *1*, 136−140.
(37) Zheng, Q.; Huang, J.; Sarjeant, A.; Katz, H. E. Pyromellitic Diimides: Minimal Cores for High Mobility n-Channel Transistor Semiconductors. *J. Am. Chem. Soc.* **2008**, *130*, 14410−14411.
(38) Ciesielski, A.; Cadeddu, A.; Palma, C.-A.; Gorczynski, A.; Patroniak, V.; Cecchini, M.; Samorì, P. Self-templating 2D supramolecular networks: a new avenue to reach control over a bilayer formation. *Nanoscale* **2011**, *3*, 4125−4129.
(39) Yoosaf, K.; Llanes-Pallas, A.; Marangoni, T.; Belbakra, A.; Marega, R.; Botek, E.; Champagne, B.; Bonifazi, D.; Armaroli, N. From Molecular to Macroscopic Engineering: Shaping Hydrogen-Bonded Organic Nanomaterials. *Chem. − Eur. J.* **2011**, *17*, 3262−3273.
(40) Đorđević, L.; Marangoni, T.; Miletic, T.; Rubio-Magnieto, J.; Mohanraj, J.; Amenitsch, H.; Pasini, D.; Liaros, N.; Couris, S.; Armaroli, N.; Surin, M.; Bonifazi, D. Solvent Molding of Organic Morphologies Made of Supramolecular Chiral Polymers. *J. Am. Chem. Soc.* **2015**, *137*, 8150−8160.
(41) Balakrishnan, K.; Datar, A.; Oitker, R.; Chen, H.; Zuo, J. M.; Zang, L. Nanobelt self-assembly from an organic n-type semiconductor: Propoxyethyl-PTCDI. *J. Am. Chem. Soc.* **2005**, *127*, 10496−10497.
(42) Kim, D. H.; Lee, D. Y.; Lee, H. S.; Lee, W. H.; Kim, Y. H.; Han, J. I.; Cho, K. High-mobility organic transistors based on single-crystalline microribbons of triisopropylsilylethynl pentacene via solution-phase self-assembly. *Adv. Mater.* **2007**, *19*, 678−682.
(43) De Luca, G.; Treossi, E.; Liscio, A.; Mativetsky, J. M.; Scolaro, L. M.; Palermo, V.; Samorì, P. Solvent vapour annealing of organic thin films: controlling the self-assembly of functional systems across multiple length scales. *J. Mater. Chem.* **2010**, *20*, 2493−2498.
(44) Vogelsang, J.; Lupton, J. M. Solvent Vapor Annealing of Single Conjugated Polymer Chains: Building Organic Optoelectronic Materials from the Bottom Up. *J. Phys. Chem. Lett.* **2012**, *3*, 1503−1513.


DOI: 10.1021/acsomega.7b00286
*ACS Omega* 2017, 2, 1672−1678